communications biology

A Nature Portfolio journal

Article

https://doi.org/10.1038/s42003-025-07871-w

Spatial transcriptomic profiling of the human fallopian tube epithelium reveals region-specific gene expression patterns

Jared Sipes[1,2], Sagar Rayamajhi[1], Leonidas E. Bantis[3,4,5], Rashna Madan[1], Amrita Mitra[1], Rajni V. Puri[1], Mohammod Mahmudur Rahman[3], Foyez Ahmmed[3,6], Harsh B. Pathak[1,5] & Andrew K. Godwin[1,2,4,5]

The fallopian tube (FT) plays a crucial role in fertility, gynecological health, and high-grade serous ovarian cancer (HGSOC) development. Despite its importance, the spatial transcriptome of the FT's distinct anatomical regions (fimbria, infundibulum, ampulla, and isthmus) remains underexplored. Using the GeoMx Digital Spatial Profiler (DSP) and a targeted ~1800 gene panel, we analyze premenopausal FT epithelium, identifying region-specific gene expression patterns. Our analysis reveals upregulation of mature ciliated cell markers (*FOXJ1*, *MLF1, SPA17, and CTSS*) approaching the fimbria, elevated ROS and apoptosis-related transcripts (*TXNIP*, *PRDX5, BAD, GAS1)* in the distal FT, and a switch in cell-cell adhesion transcripts (*CDH1*, *CDH3*) along the distal-to-proximal axis. We also provide evidence that MHC-II transcripts in the FT are differentially regulated throughout the menstrual cycle, with lower expression in follicular phase. These results suggest spatially regulated expression of FT transcripts with implications for fertilization and early neoplastic changes contributing to HGSOC.

Pathologies of the human fallopian tube (FT) are estimated to be responsible for approximately one-third of infertility cases[1,2] and tubal inflammation and obstruction are the primary cause of ectopic pregnancy. In addition, the most aggressive and lethal gynecological malignancy[3], high-grade serous ovarian cancer (HGSOC), has been linked to serous tubal intraepithelial carcinoma (STIC) lesions in the human fallopian tube epithelium (FTE)[4–6]. A growing body of evidence has accumulated supporting a link between the FTE and HGSOC, including shared mutations and chromosomal alterations between lesions and cancer[7–9], transcriptomic and proteomic comparisons showing similarities to the fallopian tube epithelium[10–13], biological studies demonstrating that normal fallopian tube epithelium undergoes oncogenic transformation upon induction of common HGSOC mutations[14], and clinical studies showing that salpingectomy reduces HGSOC incidence[15,16]. Although some HGSOC likely originates in the ovarian surface epithelium[10,14,17–20], the FTE clearly plays a significant role in the pathogenesis of this disease.

The different anatomical regions of the fallopian tube play a key role in its biological function and pathology. Moving distally to proximally, the fallopian tube is divided into five regions: 1) The fimbria, or finger-like folds surrounding the ovary which capture the released oocyte, 2) the cone-shaped infundibulum to which the fimbria are attached, 3) the ampulla, the widest section of the fallopian tube and the site of most fertilization, 4) the narrow isthmus, which transports the zygote to the uterus, and 5) the uterine part of the fallopian tube, a short section embedded in the myometrium of the uterus, which opens at the uterine ostia into the uterine lumen[21]. The uterine part of the fallopian tube plays a role in regulation of sperm entry into the oviduct in many animals, where they are then held in the isthmic "sperm reservoir" bound to the oviductal epithelium[22]. The fallopian tube is composed of an outer serosa, a middle layer of smooth muscle, and an internal mucosal layer consisting of columnar epithelium covering a lamina propria. This epithelial layer consists of folds that become progressively more labyrinthine and complex traveling from the isthmus to the fimbria. Embryologically, the fallopian tube is derived from the Müllerian (paramesonephric) duct[21].

The fallopian tube epithelium is primarily composed of ciliated and secretory epithelial cells. These cell types are not evenly distributed; there is an observed increase in the number of ciliated cells moving along the proximal to distal axis[23]. Prior to single-cell sequencing, several rarer cell

[1]Department of Pathology and Laboratory Medicine, University of Kansas Medical Center, Kansas City, KS, 66160, USA. [2]Bioengineering Program, The University of Kansas, Lawrence, KS, 64111, USA. [3]Department of Biostatistics and Data Science, University of Kansas Medical Center, Kansas City, KS, 66160, USA. [4]The University of Kansas Cancer Center, University of Kansas Medical Center, Kansas City, KS, 66160, USA. [5]Kansas Institute for Precision Medicine, University of Kansas Medical Center, Kansas City, KS, 66160, USA. [6]Department of Statistics, Comilla University, Cumilla, 3506, Bangladesh. e-mail: agodwin@kumc.edu

types had been identified, notably the stem-like peg cell population (EPCAM + /CD44 + /ITGA6 +) and a population of basal immune cells[24], but little was known about any underlying anatomical regulation of these populations.

The distal fallopian tube is exposed to a variety of oncogenic insults from follicular fluid and ovarian secretions[25,26] and multiple studies have suggested that stem cells are upregulated in both the distal murine oviduct[27] and FT fimbria[28]. Combined, these observations may explain the increase in STIC lesions reported in the fimbria of the FT[4,5,9], emphasizing the importance of fallopian tube anatomical differences in ovarian cancer pathogenesis. Despite the different functions and pathological implications of the fallopian tube, most studies of the fallopian tube do not consider potential for anatomical differences.

Several recent papers reporting on single-cell analysis of the fallopian tube have uncovered a great deal of cellular diversity in both premenopausal[29–31] and postmenopausal[32] fallopian tubes and observed significant changes in the fallopian tube throughout the menstrual cycle[33]. Some of these papers also investigated potential transcript or cell type differences along the fallopian tube distal to proximal axis, but underlying anatomical differences were not the primary focus and the contribution of transcriptome changes to fallopian tube biology remains underexplored. Laser capture microdissection has been used to compare the fimbria and ampulla of the fallopian tube, revealing differentially expressed genes related to antioxidant, stem cell and inflammatory pathways[34]. In addition, the cell diversity revealed by single-cell sequencing, and in particular the recent identification of rare WNT7A expressing cells that maintain multipotent progenitors in the fallopian tube[35], suggests that patterning of different cell types may play a crucial role in maintenance of the FTE.

We employed spatial transcriptomics to investigate the anatomical diversity of the fallopian tube. Using NanoString's GeoMx Digital Spatial Profiler platform, we characterized the spatial distribution of ~1800 transcripts in ciliated and secretory epithelial cells across four major regions of the FTE: Isthmus, infundibulum, ampulla, and fimbria. To aid in validation of markers of interest, we divided our dataset into two cohorts – a discovery cohort consisting of fallopian tubes from 3 individuals and a validation cohort with fallopian tube samples from 4 new individuals. By using this approach, we wereable to identify and validate markers that showed significant expression changes along the fallopian tube.

We show that markers of mature ciliated cells (increased *FOXJ1/PAX8* ratio, increased *MLF1, SPA17, CTSS*, and *C6*) are elevated in the distal fallopian tube. Additionally, we demonstrate that transcripts related to reactive oxygen species (ROS) and apoptosis (*TXNIP*, *PRDX5, BAD*, and *GAS1*) are upregulated in the distal fallopian tube, while cell-cell adhesion transcripts show a switch in expression along distal-to-proximal axis. Specifically, *CDH1* (E-cadherin), *CD99*, and *LGALS3* (Galectin-3) are highly expressed in the fimbria, while *CDH3* (P-cadherin) expression peaks in the isthmus. Finally, MHCII transcripts from all three major MHC isotypes (HLA-DR, DP, and DQ) showed increased expression in the isthmus, with menstrual cycle dependent variation observed throughout the rest of the fallopian tube. By establishing a baseline spatial transcriptomic profile of the normal fallopian tube epithelium, our study provides a critical reference dataset for future research leveraging spatial transcriptomics to explore pathological changes in this tissue.

Results

Collection of Spatial Transcriptomics Data from Human Fallopian Tube Epithelium

To profile the fallopian tube along the proximal to distal axis, we collected seven tissue specimens from premenopausal patients (age 25-48, mean 39) undergoing salpingectomy for non-cancer indications unrelated to fallopian tube health. Patient characteristics are detailed in Supplementary Table 1. Samples were divided into four anatomical regions (isthmus, ampulla, infundibulum, and fimbria) (Fig. 1a). We used immunofluorescence to distinguish secretory (PAX8) and ciliated (FOXJ1) epithelial cells and selected representative segments in each anatomical region (Fig. 1b), as previously described[36]. Transcriptomes were profiled using the GeoMx Cancer Transcriptome Atlas, covering ~1800 cancer-related and cell marker transcripts. Representative regions from Patient 2 are shown in Fig. 1c–f.

For validation, the dataset was split into discovery ($n = 3$) and validation ($n = 4$) cohorts (Fig. 1a). Of 110 segments in the discovery cohort, 77 passed quality control; 74 of 94 segments passed in the validation cohort (Supplementary Table 2). Quality control and quantile normalization[37] were performed separately for both cohorts. After low abundance transcripts (detected in <10% of segments) were excluded, 1026 transcripts were retained in the discovery cohort and 999 in the validation cohort. The dataset distribution by patient, region, and cell type is shown in Fig. 1g.

Segmentation validation confirmed expected marker expression: *FOXJ1* was higher in ciliated segments (Discovery logFC: 1.73, $p = 1.6 \times 10^{-11}$; Validation logFC: 1.71, $p = 1.1 \times 10^{-11}$), while *PAX8* was higher in secretory segments (Discovery logFC: -0.58, $p = 2.91 \times 10^{-11}$, Validation logFC: -0.62, $p = 3.4 \times 10^{-15}$) (Fig. 1h). These results confirm successful segmentation of ciliated and secretory populations, enabling downstream analysis.

To assess menstrual cycle status, OVGP1 immunostaining was performed. OVGP1, a fallopian tube-specific protein involved in enhancing sperm capacitation, fertilization rate, and embryo development[38], is highly differentially expressed in the fallopian tube during the menstrual cycle[34,39,40], and can be used as a marker of menstrual cycle status[33]. OVGP1 expression peaks during late follicular phase (pre-ovulatory), and decreases in luteal phase (post-ovulatory)[34,39,40]. Similar *OVGP1* upregulation is observed during estrus (late follicular stage) in other mammalian oviducts, including sheep[41,42], cow[43], goat[44], cat[45], pig[46], baboon[47], and dog[48] oviducts, as well as sheep oviductal fluid[49]. Representative slides of all regions and patients were stained for OVGP1, summarized in Supplementary fig. 1. IHC staining indicates Patients 2 and 3 were in late follicular phase (100% epithelial cells OVGP1 +), while Patients 4 and 5 were in luteal phase (<30% cells OVGP1 +). Patients 1, 6, and 7 had intermediate expression suggesting transition between phases. By chance, the discovery cohort included two follicular phase and one transition sample, while the validation cohort contained 2 luteal-phase samples and none in follicular phase (Supplementary fig. 1A-C). One patient (Patient 6) had a previous sterilization using a Filshie clip to bilaterally constrict the FT, reflected in the OVGP1 status. Distal segments (fimbria and infundibulum) remained OVGP1 + , consistent with ovarian stimulation while proximal segments (ampulla and isthmus) were OVGP1-, reflecting lack of ovarian signaling caused by the constriction.

Transcriptomic profiling of FTE shows spatially regulated transcripts

The discovery cohort was analyzed to identify differentially expressed genes (DEGs) between regions. Pairwise comparisons were performed comparing ciliated and secretory cells in each anatomical region to their counterparts in all other regions to identify DEGs. Supplementary fig. 3-4 shows DEGs (p-value < 0.05, $|\log_2(FC)| > 0.5$) in all pairwise comparisons in the discovery and validation cohorts.

To pinpoint region-specific DEGs, we compared the average expression in each region to all other regions. Figure 2a-d shows volcano plots for the discovery cohort with DEGs in secretory cells of the fimbria, infundibulum, ampulla, and isthmus, with key genes summarized in Fig. 2e. Results for ciliated cells are shown in Fig. 2f-j, and equivalent validation cohort plots are provided in Supplementary fig. 5.

We identified transcripts with sequential expression along the proximal to distal axis. Transcripts were classified as increasing (higher towards the fimbria) or decreasing (higher towards the isthmus) across regions. These DEGs are listed in Supplementary Tables 3–6.

We performed Gene Ontology analysis on DEGs identified by pairwise comparison across fallopian tube regions (Supplementary fig. 2). In secretory cells, genes differentially expressed in the fimbria versus isthmus were

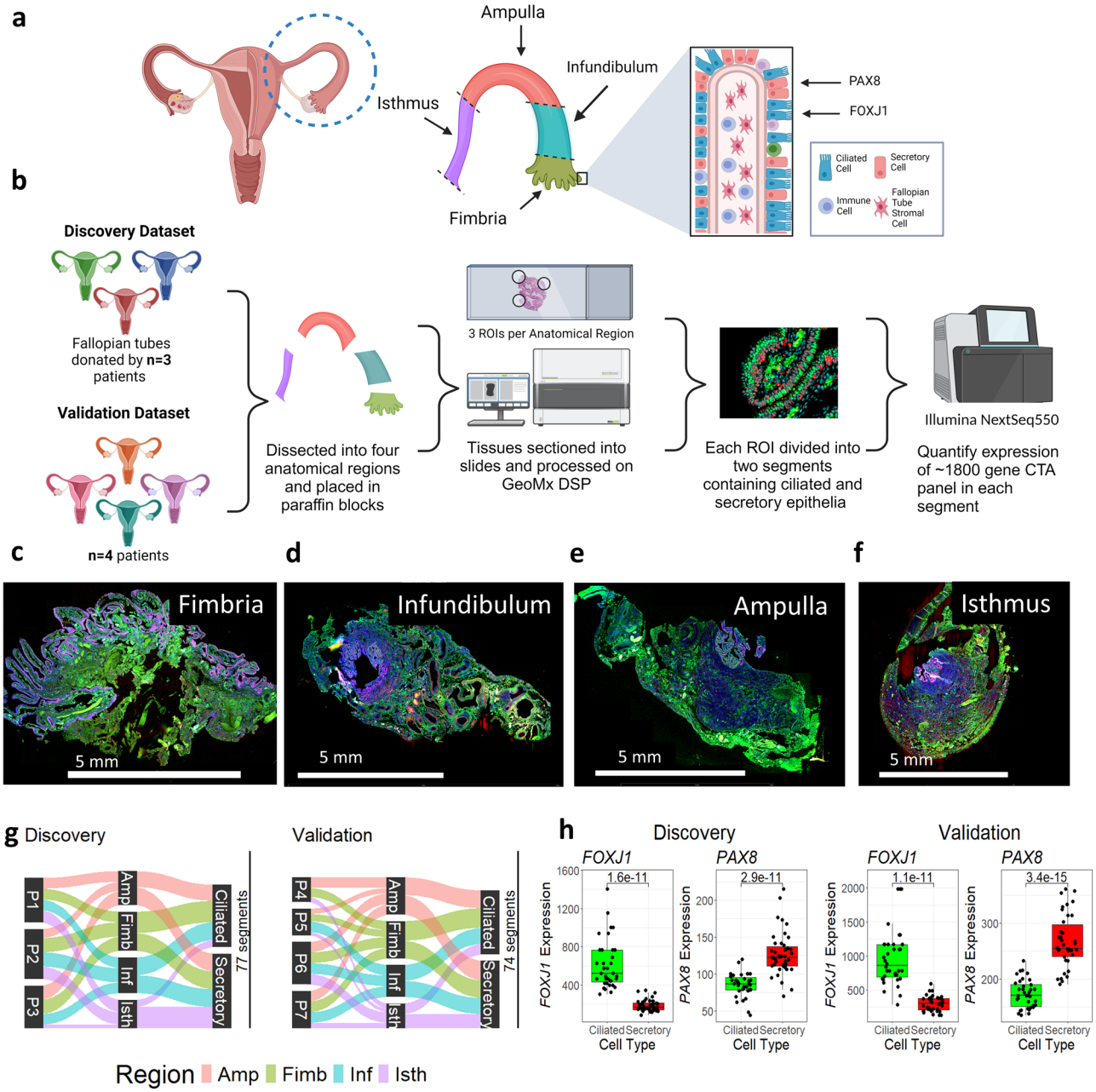

Fig. 1 | Experimental design. a Anatomy of the fallopian tube, showing the four major anatomical regions and major cell types. The transcription factors PAX8 and FOXJ1 are used to distinguish secretory and ciliated cells. **b** Experimental workflow, showing creation of discovery ($n = 3$) and validation ($n = 4$) cohorts. Following dissection into anatomical regions, regions of interest (ROIs) containing epithelial cells were selected, segmented by cell type, and probe barcodes were collected from each segment. Barcodes were sequenced on the Illumina NextSeq550, and the final output was transcript abundance for all transcripts in the ~1800-gene CTA panel. **c–f** Representative scans of the fimbria, infundibulum, ampulla, and isthmus from patient 2, showing staining and ROI selection. Nuclei (blue) = SYTO13; FOXJ1 expressing ciliated cells (green) = CY3, PAX8 expressing secretory cells (red) = AF594; Scale bar = 5 mm. **g** A Sankey diagram showing distribution of segments in the discovery and validation datasets across three categories: patient of origin, anatomical region (Amp = Ampulla (red), Fim = Fimbria (green), Inf = Infundibulum (blue), Isth = Isthmus (purple)), and cell type (ciliated or secretory). A total of 77 segments (out of 110 originally collected) remain following quality control. **h** Boxplot showing expression of *FOXJ1* and *PAX8* in ciliated and secretory segments for discovery ($n = 77$ segments) and validation ($n = 74$ segments) datasets. Ciliated = green, Secretory = red; Lower and upper hinges of boxplot correspond to first (Q1) and third quartiles (Q3); central line corresponds to median. Whiskers of boxplot range from Q3 + 1.5*IQR to Q1-1.5*IQR. *P*-values calculated using two-sided t-test. Created in BioRender. Sipes, J. (2025) https://BioRender.com/a22y908.

related to tissue development (nGenes = 15, FDR = 5.48 × 10^-8), epithelium development (nGenes = 12, FDR = 6.00 × 10^-5), apoptotic process (nGenes = 12, FDR = 0.004), and cell death (nGenes = 13, FDR = 0.003). Additionally, genes involved in the response to oxygen-containing compounds were differentially expressed between the infundibulum and isthmus (Supplementary fig. 2e). Immune-related pathways, including cytokine signaling (fimbria versus ampulla) and lymphocyte proliferation (fimbria versus infundibulum), were significantly enriched.

Since repeated ROS exposure from follicular fluid is hypothesized to contribute to early HGSOC development[25], an understanding of fallopian tube response to ROS and regulation of apoptosis may provide important information about the early development of ovarian cancer. Based on these

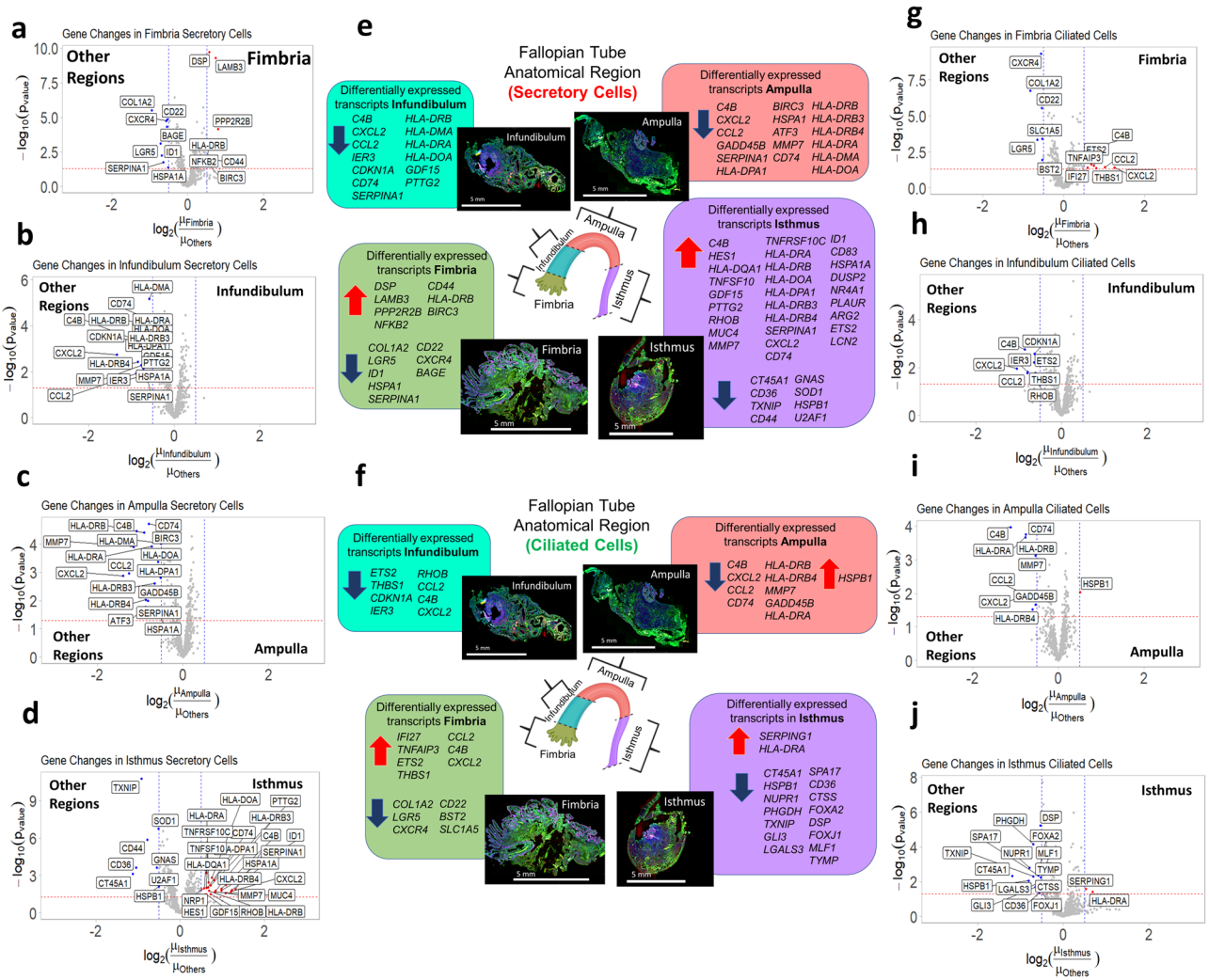

Fig. 2 | Regional comparison volcano plots showing transcripts upregulated and downregulated in secretory and ciliated ROIs in the discovery cohort. Volcano plots for secretory cell segments showing transcripts differentially expressed in **(a)** the fimbria, **(b)** the infundibulum, **(c)** the ampulla, and **(d)** the isthmus relative to all other regions. **e)** A summary of all transcripts observed upregulated and downregulated in the fallopian tube. Scale bar = 5 mm **f)** A summary of all transcripts observed upregulated and downregulated in ciliated cells. Scale bar = 5 mm **g-j)** Volcano plots for ciliated cell segments showing transcripts differentially expressed in **(g)** the fimbria, **(h)** the infundibulum, **(i)** the ampulla, and **(j)** the isthmus relative to all over regions. Red points: upregulated transcripts; blue points: downregulated transcripts, red lines: *p*-value cutoff ($-\log_{10}(p) = 1.3$); blue lines = FC cutoff ($\log_2(FC) = +/- 0.5$). Created in BioRender. Sipes, J. (2025) https://BioRender.com/p37o480.

findings, we focused on DEGs of distinct fallopian tube cell types, as well as transcripts related to ROS and immune response. To further investigate cellular differentiation across the FT, we analyzed markers of mature ciliated and secretory cells across anatomical regions.

Markers of mature ciliated cells show increased expression in the distal FTE

In the discovery cohort, fallopian tube cell type markers (FOXJ1, PAX8) showed anatomical regulation (Fig. 3a): *FOXJ1* expression was higher in ciliated cells approaching the fimbria ($p = 0.011$), while *PAX8* was lower ($p = 0.0065$; Supplementary fig. 5A-B). These transcription factors control cell-differentiation in the FT epithelium; during the secretory-to-ciliated transition, *PAX8* is downregulated while *FOXJ1* is upregulated, with immature transitional ciliated cells coexpressing both markers[31]. We used a set of mature ciliated cell markers identified by single-cell sequencing[31] and compared expression in the fimbria and isthmus (Fig. 3b).

Additionally, we conducted a sequential analysis along the proximal to distal axis, comparing the expression in the fimbria versus infundibulum, infundibulum versus ampulla, and ampulla versus isthmus (Supplementary fig. 6C-E). All comparisons, except for the infundibulum versus ampulla comparison (which had similar expression patterns), revealed increased expression of mature ciliated cell markers in the distal segment approaching the fimbria.

FOXJ1/*PAX8* expression ratios in ciliated cells (Fig. 3d) increased ($p = 0.0051$) approaching the fimbria, while *PAX8*/*FOXJ1* ratios in secretory cells (Fig. 3e) were higher approaching the isthmus ($p = 0.004$). This finding suggests that more mature ciliated cells and transitional secretory cells are found in the fimbria compared to the isthmus. Additional mature ciliated cell markers, including ciliogenesis-related[50] *MLF1* ($p = 0.00076$), *SPA17* ($p = 0.0029$), CTSS ($p = 0.0066$), and *C6* ($p = 0.067$) also increased near the fimbria, with weaker trends in secretory cells (Fig. 3f–i).

The validation cohort confirmed these results. Once again, markers of mature ciliated cells were enriched in the fimbria compared to the isthmus (Fig. 3c). In the validation dataset, *FOXJ1* expression once again increased approaching the fimbria (Supplementary fig. 6B). Ratios of *FOXJ1*/*PAX8* in ciliated cells, *PAX8*/*FOXJ1* in secretory cells, and expression of *MLF1*, *SPA17, CTSS*, and *C6* were all increased approaching the fimbria (Fig. 3j-o).

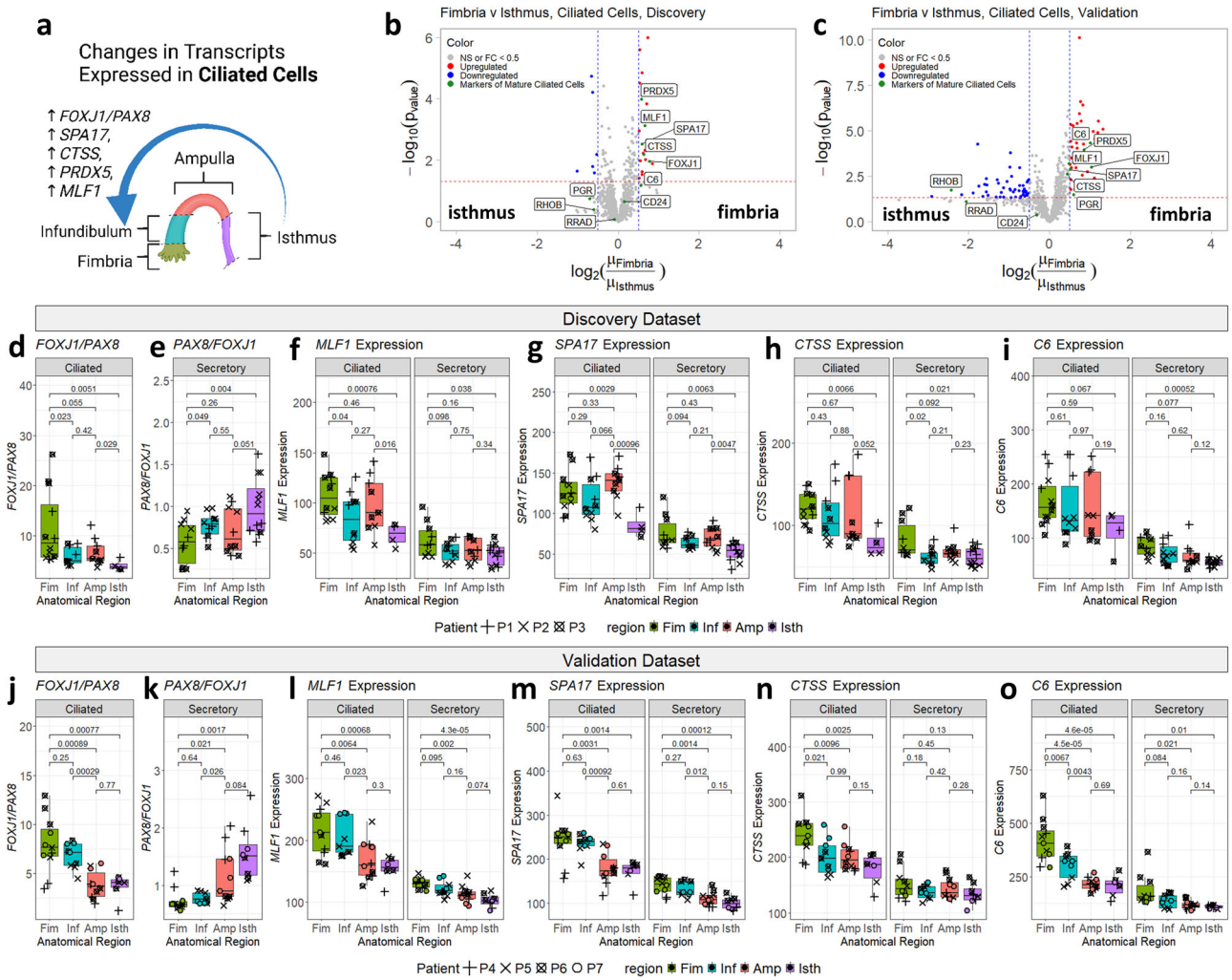

Fig. 3 | Markers of mature ciliated cells are enriched approaching the fimbria. **a** Diagram showing differential expression of markers of mature ciliated cells along the fallopian tube. Volcano plots comparing expression of transcripts between fimbria and isthmus sections in the discovery **(b)** and validation **(c)** cohorts, with mature ciliated cell markers[31] highlighted in green. Red lines: *p*-value cutoff ($-\log_{10}(p) = 1.3$); blue lines = FC cutoff ($\log_2(FC) = +/- 0.5$). All *p*-values are calculated using *t*-test.) **d** Boxplot showing ratio of FOXJ1:PAX8 ratio in ciliated cells (discovery cohort, $n = 35$). **e** Boxplot showing PAX8:FOXJ1 ratio in secretory cells (discovery cohort, $n = 42$). Boxplots showing expression of mature ciliated cell markers *MLF1* **(f)**, *SPA17* **(g)**, *CTSS* **(h)**, and *C6* **(i)** in ciliated and secretory segments (discovery cohort). **j-o** Boxplots plotting the same ratios or gene expression changes as **(d-i)**, but for the validation cohort ($n = 36$ ciliated and $n = 38$ secretory segments). Respectively, *PAX8:FOXJ1* ratio in ciliated cells **(j)**, *PAX8:FOXJ1* ratio in secretory cells **(k)**, *MLF1* expression **(l)**, *SPA17* expression **(m)**, *CTSS* expression **(n)**, and *C6* expression **(o)**. Lower and upper hinges of boxplot correspond to first (Q1) and third quartiles (Q3); central line corresponds to median. Whiskers of all boxplots range from Q3 + 1.5×IQR to Q1-1.5×IQR. All *p*-values calculated using two-sided *t*-test. Created in BioRender. Sipes, J. (2025) https://BioRender.com/p37o480.

These findings demonstrate consistent enrichment of mature ciliated cells markers toward the distal fallopian tube.

Genes involved in cell-cell adhesion are differentially expressed along the fallopian tube axis

Cell-cell adhesion genes (*CDH1*, *CDH3*, *LGALS3*, and *CD99*) are differentially expressed across the fallopian tube. *CDH1* (E-cadherin), a tumor suppressor gene frequently downregulated in cancer[51], increased distally, peaking in the fimbria (Fig. 4a). By contrast, *CDH3* (P-cadherin) shows the opposite pattern, with higher expression approaching the isthmus (Fig. 4b), perhaps reflecting a change in cell-ECM interactions along the fallopian tube. (It should be noted that even in the isthmus, *CDH3* transcripts still have lower overall expression compared to *CDH1* transcripts). Two other transcripts involved in cell-cell adhesion showed differential expression: *LGALS3* (Galectin-3) and *CD99* (MIC2) increase toward the distal fallopian tube in both secretory and ciliated cells (Fig. 4c, d). The validation cohort confirmed these trends, showing similar patterns of adhesion gene regulation along the distal to proximal axis (Fig. 4e-h).

Genes involved in ROS and apoptosis are upregulated in the distal FTE

Genes involved in oxidative stress response (*TXNIP, PRDX5*) and apoptosis (*BAD*, *GAS1*) show distinct spatial expression in the fallopian tube. *PRDX5*, encoding the antioxidant enzyme Peroxiredoxin-5, is upregulated in ciliated cells near the fimbria, with a similar but weaker trend observed in secretory cells (Fig. 4i). *TXNIP*, encoding Thioredoxin Interacting Protein, is significantly downregulated in the isthmus across both cell types (Fig. 4j).

Apoptosis-related genes also exhibit spatial regulation. *BAD* (BCL2-associated agonist of cell death) is a promoter of cell death[52] which is upregulated approaching the fimbria in secretory, but not ciliated cells (Fig. 4k). Similarly, *GAS1* (Growth Arrest Specific 1), which promotes cell cycle arrest and apoptosis, is upregulated in secretory cells approaching the fimbria (Fig. 4l).

The validation cohort corroborated these findings for *PRDX5* and *TXNIP*, revealing a consistent pattern of reduced expression in the isthmus relative to the fimbria (Fig. 4m-n). However, while the discovery dataset showed equivalent expression of these genes in the fimbria, infundibulum,

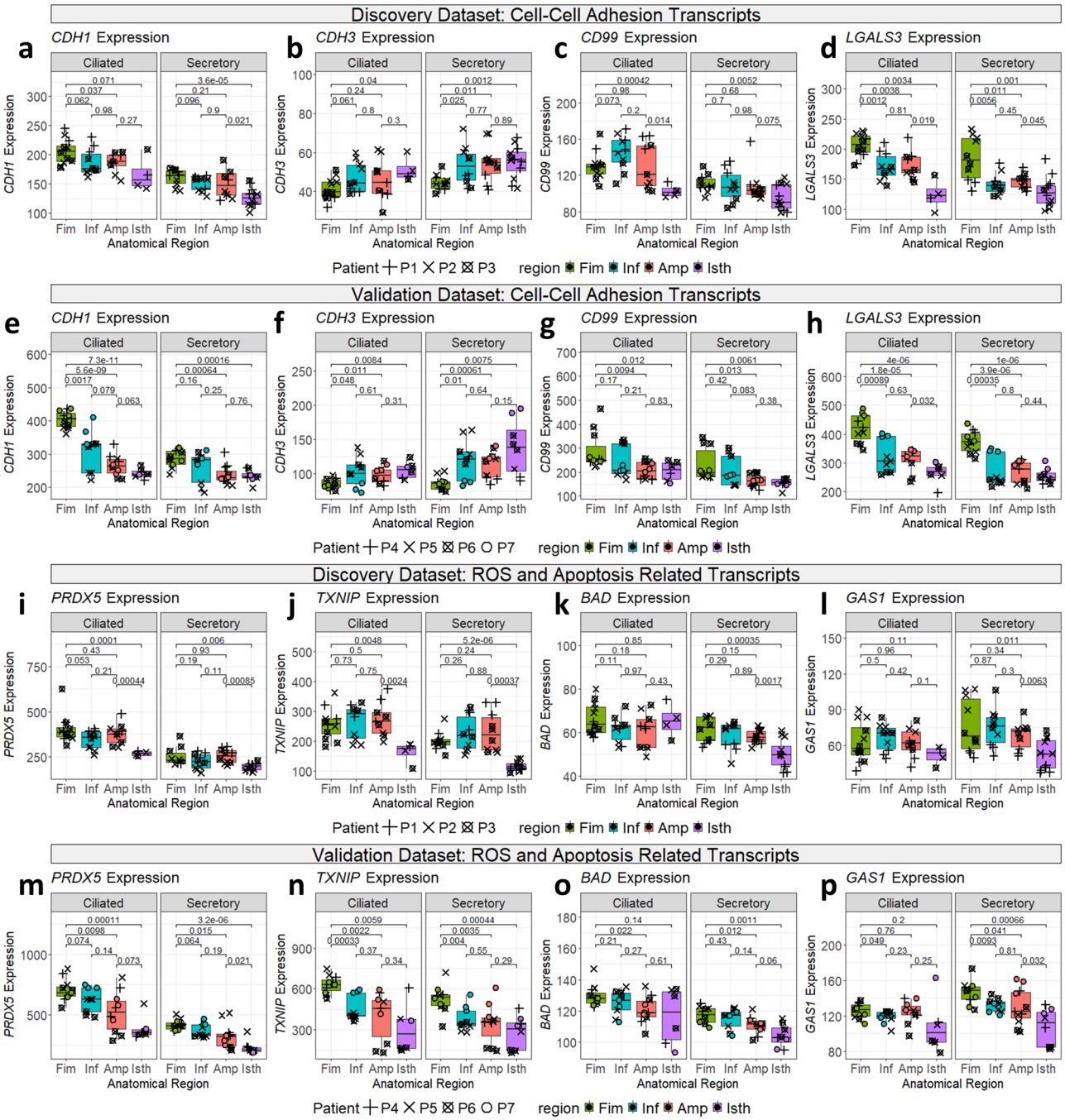

Fig. 4 | Differential expression of transcripts involved in cell-cell adhesion, ROS response, and apoptosis. a–p Boxplots of transcripts differentially expressed in different anatomical regions of the fallopian tube, showing expression in both ciliated and secretory segments. Point shapes are chosen based on patient information. *P*-values for selected comparisons are plotted. All *p*-values are calculated using two-sided *t*-test. green: fimbria; blue: infundibulum, red: ampulla, purple: isthmus; circles: pt_1, squares: pt_2, diamonds: pt_3, Lower and upper hinges of boxplot correspond to first (Q1) and third quartiles (Q3); central line corresponds to median. Whiskers of boxplot range from Q3 + 1.5*IQR to Q1-1.5*IQR. Plots (**a–h**) show cell-cell adhesion transcripts expressed in the fallopian tube epithelium in the discovery ($n = 77$) (**a–d**) and validation cohorts ($n = 74$) (**e–h**). Plots (**i–p**) show transcripts associated with reactive oxygen species or apoptosis/cell cycle expressed in the fallopian tube epithelium in the discovery (**i–l**) and validation cohorts (**m–p**).

and ampulla, the validation dataset demonstrated a linear increase toward the fimbria. Notably, the validation samples were mostly in luteal phase, as indicated by OVGP1 staining, so this potentially reflects an adaptive response to ROS exposure from follicular fluid. Similar trends were observed for *BAD* and *GAS1*, confirming their fimbrial upregulation in secretory cells (Fig. 4o-p). These findings suggest segment-specific regulation of oxidative stress and apoptotic pathways in response to environmental pressures, such as follicular fluid exposure.

MHC-II transcripts are downregulated in the interior fallopian tube during follicular phase and inversely correlated with OVGP1 expression

In the discovery cohort, MHC-II transcripts show some of the highest expression changes, with increased expression in the fimbria and isthmus compared to the ampulla and infundibulum. Although this effect was largest in secretory cells, ciliated cells show a similar trend. All three MHC-II isotypes (HLA-DR, HLA-DP, HLA-DQ) showed similar expression changes.

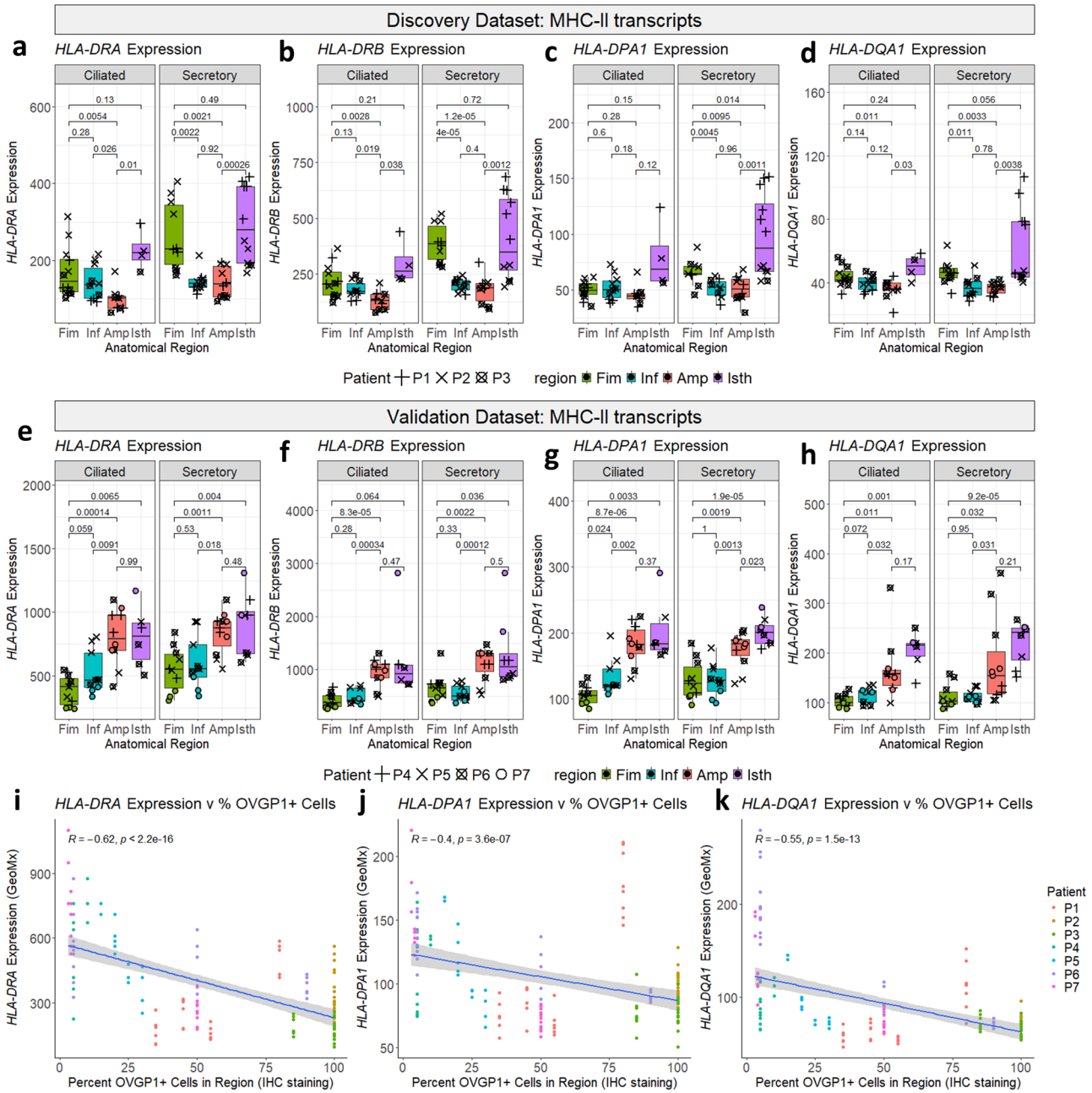

Fig. 5 | Differential expression of MHC-II and related transcripts. a-d Boxplots of MHCII transcripts differentially expressed in the discovery cohort ($n = 77$ segments). **a** *HLA-DRA*, **b** *HLA-DRB*, **c** *HLA-DPA1*, **d** *HLA-DQA1*. **e-h)** Boxplots of MHCII transcripts differentially expressed in the validation cohort ($n = 74$ segments): **e** *HLA-DRA*, **f** *HLA-DRB*, **g** *HLA-DPA1*, **h** *HLA-DQA1*. All *p*-values are calculated using two-sided *t*-test. Green: fimbria; blue: infundibulum, red: ampulla, purple: isthmus; circles: pt_1, squares: pt_2, diamonds: pt_3, Lower and upper hinges of boxplot correspond to first (Q1) and third quartiles (Q3); central line corresponds to median. Whiskers of boxplot range from Q3 + 1.5 × IQR to Q1 - 1.5 × IQR. Scatterplots comparing **i** *HLA-DRA*, **j** *HLA-DPA1*, or **k** *HLA-DQA1* expression to percentage of OVGP1 positive cells in equivalent IHC stained slides. Pearson's correlation coefficient (R) and associated *p*-value are shown on scatterplots (calculated using the R package 'ggpubr'). Grey border around the line of best fit shows the 95% confidence interval.

For example, HLA-DR subunits DRα and DRβ (encoded by *HLA-DRA* and *HLA-DRB*), show higher expression in secretory cells of the isthmus and fimbria (Fig. 5a, b). Other HLA-DR isoforms (*HLA-DRB3, HLA-DRB4;* Supplementary fig. 7A-B), the HLA-DPα subunit (*HLA-DPA1*, Fig. 5c), and the HLA-DQα subunit (*HLA-DQA1*, Fig. 5d) showed the same pattern, while *HLA-DQB1* was only significantly overexpressed in the isthmus (Supplementary fig. 7C). Of these, HLA-DR transcripts (the major MHC-II isotypes) display the highest expression and the largest regional differences.

Genes involved in MHC-II peptide loading, including *HLA-DMA*, *HLA-DOA*, and *CD74*, show the same pattern, while related transcript *HLA-DMB* was only upregulated in the fimbria (Supplementary fig. 7D-G). Notably, the HLA locus has complement genes *C2*, *C4B*, and *CFB* located between the MHC-II and MHC-I loci, of which two genes (*C4B* and *CFB*) were also upregulated in these regions (Supplementary fig. 7H-I). Collectively, these findings indicate region-specific upregulation of MHC-II transcripts at the FT's ends and downregulation in its interior.

Surprisingly, the validation dataset showed that all of these MHC-II genes were upregulated only in the isthmus, rather than the isthmus and the fimbria. This trend applied to all MHC-II isotypes (HLA-DR, -DP, -DQ; Fig. 5e-h, Supplementary fig. 7J-M), their helper genes (*HLA-DMA*, *-DMB*,

-DOA, and *CD74*; Supplementary fig. 7N-Q), and complement factors (*C2*, *C4*, *CFB*; Supplementary fig. 7R-T).

We suspected this sudden shift was due to differences in MHC-II expression during the menstrual cycle. To investigate this possibility, we compared expression of MHC-II genes (*HLA-DRA*, *HLA-DPA1*, and *HLA-DQA1*) to OVGP1 status as determined by IHC staining (Fig. 5i-k). We found a strong negative correlation between OVGP1 expression and MHC-II expression (*HLA-DRA*: R = -0.62, $p < 2.2 \times 10^{-16}$, *HLA-DPA1*: R = -0.4, $p = 3.6 \times 10^{-7}$, *HLA-DQA1*: R = -0.55, $p = 1.5 \times 10^{-13}$). These results suggest that MHC-II is downregulated in the follicular phase (when OVGP1 is highest) and upregulated in the luteal phase.

To confirm this, we reanalyzed prior FT transcriptomics studies[31,34]. Laser capture microdissection data (GEO: GSE129348) revealed *OVGP1* was upregulated in the follicular phase, while MHC-II transcripts were upregulated in the luteal phase (Supplementary fig. 8A). MHC-II transcripts showed negative correlation with *OVGP1* expression (Supplementary fig. 8B). Single-cell sequencing data (GEO: GSE178101) corroborated these findings, showing that *OVGP1* high cells have low MHC-II expression, and MHC-II transcripts negatively correlate with *OVGP1* expression (Supplementary fig. 8C-D). More recently published single-cell sequencing work by Weigert et al. goes further, showing that secretory cells of the fallopian tube cluster into three categories – one group (identified as SE1 by the authors) has high expression of MHC-II genes, while two other groups (SE2 and SE3) have high expression of OVGP1[33]. The authors show that the OVGP1 expressing SE2 cells are more common pre-ovulation (follicular phase), while the MHC-II expressing SE1 cells are more common post-ovulation (luteal phase), providing further confirmation of menstrual cycle specific effects[33]. These findings suggest that MHC-II expression in the fallopian tube is cyclically regulated, with lower expression in the follicular phase when OVGP1 is abundant, likely due to changes in MHC-II expression in OVGP1-producing secretory cells.

Markers of OVGP1 producing cells are upregulated in the interior of the FT during the follicular phase

Analysis of single-cell sequencing data suggested downregulation of MHC-II in the follicular phase is linked to OVGP1-producing secretory cells, identified as peg cells by Ulrich et al.[31]. Using peg cell markers identified in this dataset[31], we compared expression across fallopian tube regions. Peg cell markers were consistently enriched approaching the ampulla, with highest expression in the interior regions (ampulla and infundibulum) and lower expression in the fimbria and isthmus (Supplementary fig. 9A-C). While our panel does not include *OVGP1*, other markers of peg cells, including *LGR5*, *NOTCH2*, *COL1A2*, and *SERINC5*, show increased expression in secretory cells approaching the ampulla and a slight decrease in expression for most samples in the isthmus (Supplementary fig. 9D-G).

However, these trends were not replicated in the validation dataset. While *NOTCH2* showed a similar but statistically insignificant trend, *LGR5* and *COL1A2* displayed no clear trend, while *SERINC5* showed increased expression in the fimbria (Supplementary fig. 9H-K). The validation cohort had low OVGP1 immunohistochemistry expression, perhaps explaining why peg cell markers no longer display the same trends. These findings suggest OVGP1+ peg cells are enriched in the ampulla and infundibulum during follicular phase (when OVGP1 production peaks), and return to lower levels during luteal phase.

Hormone receptor expression across the fallopian tube varies with menstrual cycle status and OVGP1 expression

Steroid hormone receptors are crucial to fallopian tube function[53], influencing organogenesis and regulating gene expression. Their activity is aided by pioneer factors, which interact with condensed chromatin to enhance accessibility for hormone receptor binding[54]. In the discovery cohort, *ESR1* (estrogen receptor α) was upregulated approaching the isthmus in secretory and ciliated cells (Supplementary fig. 10A). In contrast, PGR (Progesterone Receptor) and AR (Androgen Receptor) did not show significant differences (Supplementary fig. 10B-C). Pioneer factors implicated in *ESR1* signaling also varied: *PBX1* expression increased approaching the isthmus in both cell types, while *FOXA2* was upregulated in the fimbria, but only for ciliated cells (Supplementary fig. 10D-E).

In the validation cohort, gene expression patterns differed, likely reflecting variations in menstrual cycle status. *ESR1* expression remained uniform across the fallopian tube instead of increasing toward the isthmus (Supplementary fig. 10F). *PGR* expression increased toward the fimbria in both cell types (Supplementary fig. 10G), while *AR* continued to show no trend (Supplementary fig. 10H). Interestingly, *FOXA2* maintained higher expression near the fimbria in both cohorts (Supplementary fig. 10I), but *PBX1* expression was inconsistent (Supplementary fig. 10J). A comparison of transcript expression with OVGP1 staining showed a strong positive correlation with *PGR* expression (R = 0.48, $p = 3.6*10^{-10}$), and a weak, but significant correlation with ESR1 (R = 0.21, $p = 0.01$) (Supplementary fig. 10K-L). These findings align with reports that OVGP1+ cells express hormone receptors, particularly PGR[31]. Together, these results suggest dynamic regulation of hormone receptors and pioneer factors in the fallopian tube, driven by spatial location and menstrual cycle status.

Discussion

We applied spatial transcriptomics to reveal anatomical variations in the fallopian tube transcriptome. While earlier papers have documented increases in total ciliated cell count in the distal fallopian tube[55], we show evidence of differences in distribution of mature and immature ciliated cells along the fallopian tube. Additionally, we identify spatial regulation of cell adhesion molecules, ROS- and apoptosis-related transcripts, and MHC-II transcripts. We also provide evidence that MHC-II expression in the tubal epithelium varies throughout the menstrual cycle, inversely correlating with OVGP1 expression.

As we observed above, markers of mature ciliated cells (*FOXJ1* high, *PAX8* low, *SPA17*, *C6*, *CTSS*, and *MLF1*) increase progressively along the proximal-to-distal axis, peaking in the fimbria (Fig. 6a). Prior studies show ciliated cells originate from secretory cells[28,35,56], with transitional ciliated cells co-expressing markers of both cell types[31]. This process is regulated by estrogen, which downregulates PAX8 and upregulates FOXJ1 in both mouse oviductal[56] and human FT organoids[35], increasing ciliated cell count. Estradiol is primarily synthesized by aromatases in ovarian granulosa cells and has sequentially higher concentrations in the fallopian tube lumen approaching the ovary during all phases of the menstrual cycle[57]. These findings suggest higher estradiol concentration near the ovary drive ciliated cell maturation from transitional cells and secretory precursors.

Several cell adhesion molecule (CAM) transcripts are differentially expressed along the fallopian tube. *CDH1* (E-cadherin), is upregulated distally, while *CDH3* (P-cadherin) is enriched in the proximal FT approaching the isthmus. E- and P-cadherin are both classical cadherins, the major components of cell-cell adhesive junctions which bind to other cadherins through their extracellular domains[51]. E-cadherin, an epithelial marker, is associated with strong cell-cell adhesions, whereas P-cadherin is associated with dynamic cell adhesions (for this and other reasons, loss of E-cadherin is frequently observed in cancer). *LGALS3* (Galectin-3) is a member of the galectin-family of beta-galactoside binding proteins[58]. Like the cadherin family, it is also involved in cell-cell adhesion. The isthmus, which has a denser stromal component and less epithelium, likely requires *CDH3* for epithelial-stroma adhesion, while *CDH1* and *LGALS3* may be key for epithelial adhesion in the fimbria.

Several genes related to oxidative stress (*TXNIP*, *PRDX5*) and apoptosis (*BAD*, *GAS1*) are upregulated approaching the fimbria (Fig. 6a). Ovarian secretions such as ROS found in follicular fluid are theorized to periodically damage the FT, particularly the fimbria, promoting tumorigenesis[25]. Upregulation of anti-ROS and pro-apoptosis genes may therefore represent a response to increased ROS-induced stress in these regions. *PRDX5*, an antioxidant thioredoxin protein[59], is a negative survival marker in ovarian cancer[60,61]. Impaired expression of PRDX5 is associated with inhibition of ciliogenesis and ciliopathies[62], suggesting that it may play a

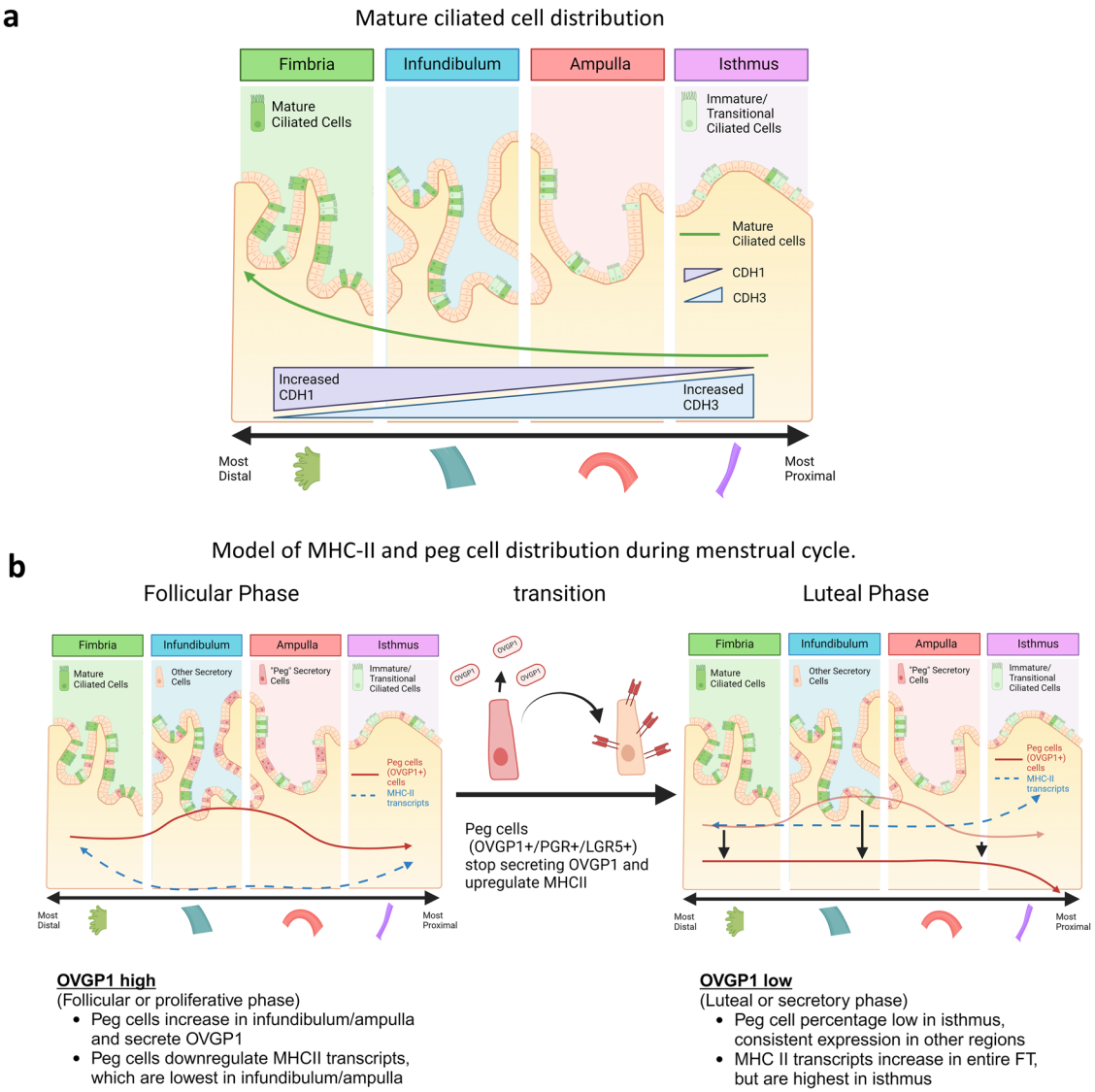

Fig. 6 | Schematic representation of cell-type distribution along the fallopian tube. a Spatial transcriptomics profiling shows that the proportion of mature ciliated cells (green line) increases approaching the isthmus. *CDH1* (E-cadherin) increases approaching the fimbria, while *CDH3* (P-cadherin) expression increases approaching the isthmus. Created in BioRender. Sipes, J. (2025) https://BioRender.com/f36o257. **b** The fallopian tube undergoes a shift in peg cell (OVGP1 +) distribution in timing with the ovulatory cycle. Pre-ovulation (follicular/proliferative phase), OVGP1 is upregulated, while MHC-II associated genes are suppressed, with the strongest effect in the central fallopian tube (infundibulum/ampulla). Post-ovulation (luteal/secretory), peg cells revert to normal secretory cells, and MHC-II genes return to a higher expression throughout the fallopian tube, with the isthmus showing the highest overall expression. MHC-II transcripts (blue, dotted line) show an increase approaching the isthmus. Dark green cell with cilia = mature ciliated cells; light green cell with cilia = immature/transitional ciliated cells. Created in BioRender. Sipes, J. (2025) https://BioRender.com/k86a54.

similar role in fallopian tube ciliated cells, where it is strongly upregulated relative to secretory cells. *TXNIP*, in contrast, actually has *pro*-oxidant function[63] by inhibiting thioredoxin proteins. While normally residing in the nucleus, under conditions of excessive oxidative stress, TXNIP transfers out of the nucleus and binds to TRX1 or TRX2, preventing them from inhibiting ASK1 and inducing apoptosis[64]. BAD, also known as Bcl-2 associated agonist of cell death, is involved in activation of the mitochondrial "intrinsic apoptosis pathway"[52] through inhibition of anti-apoptotic proteins in the Bcl-2 family proteins. This leads to activation of pro-apoptotic proteins like BAX and BAK, which oligomerize and promote mitochondrial permeability, leading to apoptosis. BAD expression is reduced in ovarian cancer[65], suggesting that disruption of this pathway may be involved in ovarian cancer development. Another apoptosis-related transcript upregulated in the distal fallopian tube, GAS1 (Growth Arrest Specific 1) is associated with cell cycle arrest in the G0 to S transition[66] and induces dephosphorylation of BAD, promoting its pro-apoptotic functions[67]. The upregulation of *TXNIP*, *GAS1*, and *BAD* approaching the distal FT suggests that a higher percentage of fimbrial cells are either undergoing apoptosis or sensitized to apoptotic signals, perhaps in response to stress from follicular fluid. Together, upregulation of ROS responsive proteins like PRDX5 may increase resistance to oxidative follicular fluid in the fimbria, while pro-apoptotic proteins like TXNIP, BAD, and GAS1 may eliminate cells with irreparable ROS damage, providing a protective function in the distal FT.

MHC-II (Major Histocompatibility Complex II) transcripts were among the most differentially expressed in the FT. MHC-II presents extracellular peptide antigens to CD4 + T cells[68], a process typically mediated by professional antigen presenting cells (APCs). However, non-professional APCs, including epithelial cells of the gastrointestinal and respiratory tracts[69], also present MHC-II. There are three MHC-II isotypes: HLA-DR, -DP, and -DQ. During MHC-II synthesis in the endoplasmic reticulum, the invariant chain (CD74) binds to MHC-II, preventing self-peptide binding and directing MHC-II to the endosome, where HLA-DM

removes CD74 and loads non-self peptides. HLA-DO regulates HLA-DM activity[68].

In the FT, MHC-II shows region-specific regulation inversely correlated with OVGP1, leading us to suggest a potential model of OVGP1+ secretory cell distribution influenced by both anatomical region and menstrual cycle status (Fig. 6b). High OVGP1 expression (follicular phase) coincides with low MHC-II levels, particularly in the infundibulum and ampulla. Conversely, during luteal phase, OVGP1 decreases while MHC-II increases, peaking in the isthmus. This pattern aligns with findings that peg cells, a secretory subpopulation expressing >30x higher OVGP1 than other FT cells, exhibit minimal MHC-II expression[31,33]. Thus, peg-cell distribution may explain MHC-II regulation across FT regions, although further functional studies are needed to confirm this model.

We observed that peg-cell markers (*LGR5*, *NOTCH2*, and *COL1A2*) increase approaching the ampulla (Fig. 6) in FT samples with high OVGP1 expression (discovery dataset). However, there is no clear trend in OVGP1-low samples, likely due to fewer peg cells. This was surprising, since previous work has suggested that peg cells were more common in the fimbria[28]. Since peg-like cells increase pre-ovulation and decrease post-ovulation[33], estrogen may promote peg cell differentiation, while progesterone reduces it. While estradiol signaling alone would predict peg-cell enrichment near the fimbria, the observed distribution toward the ampulla suggests additional regulatory factors. This distribution may optimize the FT microenvironment for fertilization, as OVGP1 – a major peg cell product – enhances fertilization rate and early embryonic development[38], the early stages of which take place in the ampulla.

The downregulation of MHC-II by OVGP1-expressing cells may create an immunosuppressed microenvironment, preventing antigen presentation of sperm or zygote-derived peptides to CD4 + T-cells. Immunotolerance of the embryo is crucial to successful pregnancy[70] and it is possible that MHC-II regulation in the FT mediates this process. While mucosal epithelial cells are not professional APCs, they can present antigens under specific conditions[69]. Infection or inflammation can induce costimulatory molecules like CD80, CD86 and CD40 in the respiratory and gastrointestinal epithelium, enabling T cell activation[71,72]. Epithelial cells can transfer MHC-II/peptide complexes through extracellular vesicles (EVs) to APCs, which can efficiently activate T cell responses[73,74]. Conversely, epithelial MHC-II can also promote immunotolerance. In intestinal epithelium models, MHC-II knock-out exacerbated colitis[75] and intestinal epithelial cells promoted T reg differentiation via MHC-II[76]. A similar dual role may exist in the hFTE, with MHC-II either supporting or inhibiting host immune response.

Complicating this analysis, the precise timing of OVGP1 downregulation and MHC-II upregulation during early pregnancy remains unclear. Would OVGP1+ cells persist post-fertilization, suppressing MHC-II or would MHC-II upregulation aid maternal immune tolerance via regulatory T cells? Strong menstrual cycle regulation of MHC-II suggests a reproductive role, warranting further research to elucidate these mechanisms.

Our study has several limitations. Although we tried where possible to capture similar sized ROIs, the size difference between the fimbria and isthmus made this difficult. To mitigate technical bias, we applied quantile normalization, shown to improve correction for differences in signal-to-noise ratio compared to alternatives in GeoMx DSP datasets[37]. Furthermore, this proof of principle study is limited by sample size and subject to effects from patient variability. To address this, we divided the dataset into two cohorts, using one for validation. The panel used for this study is also limited, as we employed a cancer-focused panel instead of expanded transcriptome (*i.e.*, ~ 18,000 genes), which could have provided additional insights. Future work with single-cell spatial workflows will likely uncover new cell-cell signaling networks that regulate epithelial structure.

It is recognized that menstrual cycle effects significantly influence FT biology. Thoroughly addressing this confounder would require profiling multiple samples from each phase of the cycle. By staining for OVGP1, we show that our fallopian tube samples were collected across various cycle stages and that most of the effects observed -- except for MHC-II transcript and peg-cell transcript expression -- are independent of menstrual cycle status. Use of hormonal birth control may also affect the FT transcriptome, but FT samples from patients not on birth control are rare (only one of seven in our dataset). This fallopian tube (from patient 6) was also unique because of previous sterilization using a Filshie clip to restrict the fallopian tube. This has the potential to modify the normal FT transcriptome; however, removal of this sample from the dataset did not change our conclusions, with the sole exception that *CDH3* upregulation in the isthmus in the validation dataset was no longer significant due to the smaller sample size.

Further research will determine how the FT transcriptome varies with menstrual cycle phase, age, hormonal contraceptive usage, and *BRCA1/2* mutation status to better understand the role of anatomical variation in reproductive biology and the origins of high-grade serous ovarian cancer in the fallopian tube. Overall, we believe that this study provides new and useful information regarding the basic biology of the fallopian tube and its anatomically regulated gene expression profile that can support a better understanding of function and susceptibility to cancer development.

In summary, we demonstrate differential anatomical regulation of key transcripts related to ROS, apoptosis, and MHC-II antigen display in the FT. We show evidence of anatomical distribution of multiple cell-types identified through single-cell sequencing and show that peg-cell distribution may be linked to a local decrease in MHC-II expression in the interior FT. Our findings provide a baseline for future spatial transcriptomics studies to further explore FT function and pathology.

Methods

Human specimen collection procedures

This study follows the guidelines of the University of Kansas Medical Center (KUMC) research ethics committee. All experiments are performed in accordance with the standards laid down by the 1964 Declaration of Helsinki and later amendments. Human specimen collection approval was obtained by the KUMC Institutional Review Board under the existing Biospecimen Repository Core Facility protocol (HSC #5929). Study coordinators approached women who met the study criteria during the office visit or surgical appointment. The study coordinators obtained written informed consent from each patient participant prior to study enrollment. Fallopian tube tissue specimens were obtained from consenting women undergoing non-cancer related surgeries for either a permanent form of birth control or for conditions not directly involving the fallopian tube, e.g., help prevent cancer, an ectopic pregnancy, or endometriosis, and de-identified in accordance with KUMC procedures before being used for research studies. All ethical regulations relevant to human research participants were followed.

Relevant medical information related to the three samples collected for the current study is contained in Supplementary Table 1. Patients ranged from 30 to 48 years in age and, based on age and medical information provided, were either pre- or peri-menopausal. All patients, with the exception of patient 6, used hormonal birth control at the time of or shortly prior to surgery, details of which are given in Supplementary Table 1. No diagnostic abnormalities were identified in the fallopian tube samples.

Whole fallopian tube samples from salpingectomies were inspected by a pathology assistant (PA) and the different anatomical regions were identified as follows. The distal and proximal ends of the fallopian tube were identified, and the dimensions of the tube were recorded. The fallopian tube was divided near the midpoint of the tube, between the regions judged by the PA to be the ampulla and infundibulum (resulting in one proximal fimbria-infundibulum segment and one distal ampulla-isthmus segment). The two resulting segments were then divided at approximately their midpoints by the PA, resulting in four segments (from most distal to most proximal): fimbria, infundibulum, ampulla, and isthmus. Each region was fixed in 10% formaldehyde for 24 h, followed by transfer to ethanol gradients, then embedded in paraffin with labels identifying the anatomical region for future sectioning. Presence of epithelium was confirmed by hematoxylin and eosin (H&E) staining of the sectioned tissue. Three

adjacent sections of fallopian tube tissue from each segment were placed on the same slide within the boundaries required for the GeoMx DSP.

Immunohistochemistry staining of OVGP1

For OVGP1 staining, a rabbit polyclonal anti-human OVGP1 antibody was used (ThermoFisher PA5-64007, RRID: AB_2645127) at a 1:200 dilution, followed by HRP based detection kit using an anti-rabbit secondary conjugated to HRP at a concentration predefined by manufacturer. Slides were stained using the Dako Autostainer Plus S3800 Slide Stainer. Incubation times were 30 min with the primary antibody and 30 min with the secondary. Following staining, slides were reviewed by Dr. Rashna Madan, a clinical pathologist, who provided estimates of staining intensity and percentage of OVGP1+ cells.

Slide preparation for GeoMx digital spatial profiling

Formalin-fixed paraffin-embedded (FFPE) slides were prepared following the "RNA Slide Preparation Protocol" in MAN-10150 in the Manual Slide Preparation User Manual, available from NanoString. Briefly, slides were deparaffinized in xylene, followed by washing in a series of ethanol gradients. Antigen target retrieval was performed in 1x Tris EDTA in a steamer for 20 min, followed by digestion using a 1 µg/mL solution of Proteinase K in RNase free, DEPC treated water at 37 °C for 20 min to expose RNA targets. Slides were next briefly preserved in 10% NBF for 5 min, followed by washes in NBF stop buffer.

The RNA probe hybridization solution was prepared using the GeoMx® Cancer Transcriptome Atlas (CTA) RNA probe mix (NanoString), following the recommended dilution (10% probe mix + 10% DEPC water + 80% Buffer R). Sections were circled individually using a hydrophobic barrier pen, then 50 µL of the hybridization solution was applied to each tissue section. Each tissue section was covered with a HybriSlip coverslip and incubated overnight in a humidified hybridization chamber at 37 °C for approximately 16 h.

Following hybridization, unbound probes were removed by two 5 min washes at 37 °C in a 1:1 solution of 4x SSC buffer and formamide, followed by two washes in 2x SSC buffer at room temperature.

Immunofluorescence Staining of Fallopian Tube Tissue and Imaging

Following RNA-probe hybridization, slides are stained for markers of ciliated (FOXJ1) and secretory (PAX8) cells using methods we have previously described[36]. Slides were incubated for 1 h with a primary solution of 1:100 mouse anti-FOXJ1 (Invitrogen, 14-9965-82, unconjugated) and 1:50 anti-PAX8 (Proteintech, CL594-10336, conjugated with CoraLite594) in BufferW (NanoString), followed by a 30 min secondary stain containing 1:50 anti-mouse antibody (Invitrogen, A10521, conjugated to CY3) and 10% SYTO13 (nuclei stain, NanoString) in BufferW.

Stained slides were scanned on the GeoMx® DSP. Regions of Interest (ROIs) were selected in the epithelium and divided into secretory and ciliated segments based on the expression of PAX8 and FOXJ1 in the tissue sections. Segmentation is an automated process that takes place on the GeoMx, guided by user adjustment of min and max fluorescence cutoffs. Two digital masks are generated to identify regions with high CoraLite594 (*PAX8* – secretory cells) or high CY3 (*FOXJ1* - ciliated cells). Both of these markers are well validated for both secretory and ciliated cells and have been previously validated by our group for segmentation of fallopian tube epithelium on the GeoMx platform[36]. Hybridized probes from these segments were collected in a 96-well plate (details of ROI selection and collection can be found in MAN-10116-05 for the software v2.3, NanoString). Full scans of all slides for this project may be found in Supplementary Data 1.

Library prep was performed according to instructions provided in NanoString's NGS Readout Library Prep User Manual (MAN-10117-05), followed by paired-end (27 × 27 cycles) sequencing on the Illumina NextSeq 550 sequencer using a high-output flow cell. FASTQ files downloaded from the NextSeq are converted into the DCC file format using the GeoMxNGSPipeline (version-2.3.3.10).

Statistics and reproducibility

Quality control and filtering of GeoMx DSP data. Initial quality control and data analyses were performed using the GeoMxWorkflows[77], NanoStringNCTools, and GeoMxTools packages provided on Bioconductor, following the vignette "Analyzing GeoMx-NGS RNA Expression Data with GeoMxTools" provided by NanoString.

Briefly, DCC files (containing the expression count data), PKC files (containing the probe assay metadata from NanoString), and an Excel file containing segment annotation information are used to create the NanoStringGeoMxSet Object. Quality control was performed to identify segments with any of the following: <1000 reads, <80% trimmed, <80% stitched, <75% aligned, <50% saturated, <1 negative probe count, >3000 NTC count, and <20 nuclei. All flagged segments were removed from the study.

Individual probes were removed from the dataset following the probe QC if they were identified as outliers (see GeoMxWorkflows vignette for details), followed by creating the gene level count data by calculating the geometric mean of all remaining probes. Limit of quantitation was determined and segments with <10% of genes from the panel detected were filtered out, followed by removal of genes detected in <10% of segments, as recommended by NanoString.

For the full dataset and accompanying quality control workflow, please see the GitHub repository associated with this paper, archived on Zenodo[78] (https://doi.org/10.5281/zenodo.14884931). R markdown workflows and data files are also included in Supplementary Data 2. R version 4.2.3 was used for quality control and filtering data analysis.

Normalization of GeoMx DSP data. The filtered dataset consisted of 1026 transcripts and 77 segments. Each segment is labeled based on cell type (ciliated or secretory) and region of origin (fimbria, infundibulum, ampulla, or isthmus). The distribution of the segments in each group was visualized as a Sankey diagram in Fig. 1g. For details of the segment numbers for each region and subtype, see Supplementary Table 2. Each segment represents a unique measurement of RNA expression in the target capture region, not a technical replicate. The data was normalized using the quantile normalization method[37]. The quantile normalization method aligns count values according to gene rank, forcing all samples to have the same distribution. In this method, all genes in a sample are ranked based on pre-normalized count, from highest to lowest, then the normalized count is set to the mean of all counts in the same rank (for each sample, the highest transcript is assigned a new value of the mean of all the highest counts in each sample, the second highest transcript is assigned to the mean of the second highest counts, and so forth). This method has been shown to improve upon Q3 normalization, adjusted CPM, DESeq2, and gamma fit correction in correcting for potential technical bias caused by systematic differences in signal-to-noise ratio between samples[37]. The analysis was conducted using R (version 4.3.1).

Differential gene expression analysis between segments – comparison of ciliated and secretory segments. For each transcript, we conducted a two-sided *t*-test between the ciliated and secretory groups of segments. We report the corresponding *p*-value and log-fold change for each marker. We extracted two subsets of effective markers from the pool of 1026 markers based on two different criteria: Criterion 1: ($p - value < 0.05$ and $|\log_2(FC)| > 1$) and Criterion 2: ($p - value < 0.05$ and $|\log_2(FC)| > 0.5$.) A full list of transcripts differentially expressed between the two cell types is available in Supplementary Data 3.

Pairwise comparisons between anatomical regions. We compared all pairwise regions (fimbria vs infundibulum, infundibulum vs ampulla, etc.) using the two-sided unpaired *t*-test for each marker, and then identified effective markers based on the criteria mentioned above. A full list of the *p*-values and log-fold changes for each pairwise comparison may be found in Supplementary Data 4.

To identify transcripts upregulated or downregulated in a specific region versus all other regions, we compared average expression in one

region to average expression in all other regions (fimbria vs all other regions, infundibulum vs all others, etc.) using the two-sided *t*-test for each marker and identified effective markers. A full list of the *p*-values and log-fold changes for all genes, along with the DEGs in each region, may be found in Supplementary Data 5.

Identification of transcripts upregulated or downregulated along the proximal-to-distal axis. We searched for genes upregulated along the proximal-to-distal axis (higher approaching the fimbria) or downregulated along the proximal-to-distal axis (high approaching the isthmus). Initially, we grouped each marker by region and calculated the mean values for segments within each region. For each marker, we obtained 4 mean values corresponding to 4 different regions. We created two sub-groups of markers that showed ascending (fimbria < infundibulum < ampulla < isthmus) or descending (fimbria > infundibulum > ampulla > isthmus) region mean patterns. In secretory cells, 57 of the RNA transcripts showed an ascending pattern, and 39 of the markers showed a descending pattern. In ciliated cells, 56 of the RNA transcripts showed an ascending pattern, while 42 showed a descending pattern. To check to see if these patterns were significant, we first performed ANOVA to compare marker expression in the four regions, then performed a t-test to compare the two endpoints *i.e.*, pair wisely comparing Fimbria vs Isthmus.

For secretory cells, based on a 0.05 nominal level, 16 transcripts showed a significant ascending pattern and 24 markers showed a statistically significant descending pattern based on the ANOVA test. All of the secretory cell transcripts identified using ANOVA were also significant using the *t*-test.

For the ciliated cells, 13 transcripts showed significant ascending pattern and 7 showed significant descending pattern based on the ANOVA test. Comparison of the endpoints showed that 6 of the ascending and 6 of the descending ciliated group transcripts were also significant using the t-test. A table with all mRNA transcripts showing sequential increase or decrease along the proximal-distal axis may be found in Supplementary Data 6.

Packages and methods used to create graphs. All graphs were created using R-version 4.2.3. An R-markdown document with the functions and libraries used to create these graphs may be found at the Zenodo archive[78] for this project (https://doi.org/10.5281/zenodo.14884931). Transcripts identified as differentially expressed through statistical analysis may be found in Supplementary Data 3-6.

Reporting summary

Further information on research design is available in the Nature Portfolio Reporting Summary linked to this article.

Data availability

Full slide scans are available as .jpg files in Supplementary Data 1. The full spatial transcriptomics dataset and workflow may be downloaded at the GitHub repository for this project, archived in Zenodo[78] (https://doi.org/10.5281/zenodo.14884931), or from Supplementary Data 2. Lists of transcripts identified as differentially expressed may be found in Supplementary Data 3–5. The full dataset associated with this project has been uploaded to Gene Expression Omnibus, GEO: GSE290051. The laser capture microdissection dataset[34] analyzed in this study is available at the NCBI Gene Expression Omnibus, GEO: GSE129348. The spatial transcriptomics dataset[31] analyzed in this study is available at the NCBI Gene Expression Omnibus, GEO: GSE178101.

Code availability

The code used for initial filtering, quality control, and graphing is available on GitHub and archived using Zenodo[78] (https://doi.org/10.5281/zenodo.14884931). The code used for data normalization and statistical analysis is available upon request.

Received: 22 February 2024; Accepted: 3 March 2025;
Published online: 29 March 2025

References

1. Briceag, I. et al. Fallopian tubes–literature review of anatomy and etiology in female infertility. *J. Med Life* **8**, 129–131 (2015).
2. Miller, J. H., Weinberg, R. K., Canino, N. L., Klein, N. A. & Soules, M. R. The pattern of infertility diagnoses in women of advanced reproductive age. *Am. J. Obstet. Gynecol.* **181**, 952–957 (1999).
3. Ferlay, J. et al. Cancer incidence and mortality worldwide: Sources, methods and major patterns in GLOBOCAN 2012. *Int. J. Cancer* **136**, E359–E386 (2015).
4. Medeiros, F. et al. The Tubal Fimbria Is a Preferred Site for Early Adenocarcinoma in Women With Familial Ovarian Cancer Syndrome. *Am. J. Surgical Pathol.* **30**, 230–236 (2006).
5. Lee, Y. et al. A candidate precursor to serous carcinoma that originates in the distal fallopian tube. *J. Pathol.* **211**, 26–35 (2007).
6. Shih, I. M., Wang, Y. & Wang, T. L. The Origin of Ovarian Cancer Species and Precancerous Landscape. *Am. J. Pathol.* **191**, 26–39 (2021).
7. Bashashati, A. et al. Distinct evolutionary trajectories of primary high-grade serous ovarian cancers revealed through spatial mutational profiling. *J. Pathol.* **231**, 21–34 (2013).
8. Wang, Y. et al. Aneuploidy Landscape in Precursors of Ovarian Cancer. *Clin. Cancer Res.* https://doi.org/10.1158/1078-0432.Ccr-23-0932 (2023).
9. Labidi-Galy, S. I. et al. High grade serous ovarian carcinomas originate in the fallopian tube. *Nat. Commun.* **8**, 1093 (2017).
10. Lawrenson, K. et al. A Study of High-Grade Serous Ovarian Cancer Origins Implicates the SOX18 Transcription Factor in Tumor Development. *Cell Rep.* **29**, 3726–3735.e3724 (2019).
11. Coscia, F. et al. Integrative proteomic profiling of ovarian cancer cell lines reveals precursor cell associated proteins and functional status. *Nat. Commun.* **7**, 12645 (2016).
12. Beirne, J. P. et al. Defining the molecular evolution of extrauterine high grade serous carcinoma. *Gynecologic Oncol.* **155**, 305–317 (2019).
13. Lynch, H. T. et al. Hereditary ovarian carcinoma: heterogeneity, molecular genetics, pathology, and management. *Mol. Oncol.* **3**, 97–137 (2009).
14. Zhang, S. et al. Both fallopian tube and ovarian surface epithelium are cells-of-origin for high-grade serous ovarian carcinoma. *Nat. Commun.* **10**, 5367 (2019).
15. Ely, L. K. & Truong, M. The role of opportunistic bilateral salpingectomy vs tubal occlusion or ligation for ovarian cancer prophylaxis. *J. Minim. invasive Gynecol.* **24**, 371–378 (2017).
16. Kahn, R. M. et al. Salpingectomy for the Primary Prevention of Ovarian Cancer: A Systematic Review. *JAMA Surg.* **158**, 1204–1211 (2023).
17. Godwin, A. K. et al. Spontaneous Transformation of Rat Ovarian Surface Epithelial Cells: Association With Cytogenetic Changes and Implications of Repeated Ovulation in the Etiology of Ovarian Cancer. *JNCI: J. Natl. Cancer Inst.* **84**, 592–601 (1992).
18. Testa, J. R. et al. Spontaneous transformation of rat ovarian surface epithelial cells results in well to poorly differentiated tumors with a parallel range of cytogenetic complexity. *Cancer Res.* **54**, 2778–2784 (1994).
19. Godwin, A. K., Testa, J. R. & Hamilton, T. C. The biology of ovarian cancer development. *Cancer* **71**, 530–536 (1993).
20. Dyck, H. G. et al. Autonomy of the epithelial phenotype in human ovarian surface epithelium: Changes with neoplastic progression and with a family history of ovarian cancer. *Int. J. Cancer* **69**, 429–436 (1996).
21. Standring, S. in *Gray's Anatomy: The Anatomical Basis of Clinical Practice* (ed Susan Standring) (Elsevier Limited, 2021).

22. Holt, W. V. & Fazeli, A. The oviduct as a complex mediator of mammalian sperm function and selection. *Mol. Reprod. Dev.* **77**, 934–943 (2010).
23. Crow, J., Amso, N. N., Lewin, J. & Shaw, R. W. Physiology: Morphology and ultrastructure of Fallopian tube epithelium at different stages of the menstrual cycle and menopause. *Hum. Reprod.* **9**, 2224–2233 (1994).
24. Peters, W. M. Nature of "basal" and "reserve" cells in oviductal and cervical epithelium in man. *J. Clin. Pathol.* **39**, 306–312 (1986).
25. Bergsten, T. M., Burdette, J. E. & Dean, M. Fallopian tube initiation of high grade serous ovarian cancer and ovarian metastasis: Mechanisms and therapeutic implications. *Cancer Lett.* **476**, 152–160 (2020).
26. Wang, Y. et al. Identification of quiescent, stem-like cells in the distal female reproductive tract. *PLoS One* **7**, e40691 (2012).
27. Xie, Y., Park, E. S., Xiang, D. & Li, Z. Long-term organoid culture reveals enrichment of organoid-forming epithelial cells in the fimbrial portion of mouse fallopian tube. *Stem Cell Res* **32**, 51–60 (2018).
28. Paik, D. Y. et al. Stem-like epithelial cells are concentrated in the distal end of the fallopian tube: a site for injury and serous cancer initiation. *Stem Cells* **30**, 2487–2497 (2012).
29. Hu, Z. et al. The Repertoire of Serous Ovarian Cancer Non-genetic Heterogeneity Revealed by Single-Cell Sequencing of Normal Fallopian Tube Epithelial Cells. *Cancer Cell* **37**, 226–242.e227 (2020).
30. Dinh, H. Q. et al. Single-cell transcriptomics identifies gene expression networks driving differentiation and tumorigenesis in the human fallopian tube. *Cell Rep.* **35**, 108978 (2021).
31. Ulrich, N. D. et al. Cellular heterogeneity of human fallopian tubes in normal and hydrosalpinx disease states identified using scRNA-seq. *Dev. Cell* **57**, 914–929.e917 (2022).
32. Lengyel, E. et al. A molecular atlas of the human postmenopausal fallopian tube and ovary from single-cell RNA and ATAC sequencing. *Cell Rep.* **41**, 111838 (2022).
33. Weigert, M. et al. A cell atlas of the human fallopian tube throughout the menstrual cycle and menopause. *Nat. Commun.* **16**, 372 (2025).
34. Sowamber, R. et al. Integrative Transcriptome Analyses of the Human Fallopian Tube: Fimbria and Ampulla-Site of Origin of Serous Carcinoma of the Ovary. *Cancers (Basel)* **12**, https://doi.org/10.3390/cancers12051090 (2020).
35. Alsaadi, A. et al. Single-cell transcriptomics identifies a WNT7A-FZD5 signaling axis that maintains fallopian tube stem cells in patient-derived organoids. *Cell Rep.* **42**, 113354 (2023).
36. Zha, D. et al. Proteomic Profiling of Fallopian Tube-Derived Extracellular Vesicles Using a Microfluidic Tissue-on-Chip System. *Bioengineering (Basel)* **10**, 423 (2023).
37. van Hijfte, L. et al. Alternative normalization and analysis pipeline to address systematic bias in NanoString GeoMx Digital Spatial Profiling data. *iScience* **26**, 105760 (2023).
38. Zhao, Y., Vanderkooi, S. & Kan, F. W. K. The role of oviduct-specific glycoprotein (OVGP1) in modulating biological functions of gametes and embryos. *Histochem. Cell Biol.* **157**, 371–388 (2022).
39. Arias, E. B., Verhage, H. G. & Jaffe, R. C. Complementary Deoxyribonucleic Acid Cloning and Molecular Characterization of an Estrogen-Dependent Human Oviductal Glycoprotein1. *Biol. Reprod.* **51**, 685–694 (1994).
40. Briton-Jones, C. et al. Regulation of human oviductin mRNA expression in vivo. *Fertil. Steril.* **75**, 942–946 (2001).
41. Chen, W., Li, Z., Zhong, R., Sun, W. & Chu, M. Expression profiles of oviductal mRNAs and lncRNAs in the follicular phase and luteal phase of sheep (Ovis aries) with 2 fecundity gene (FecB) genotypes. *G3 (Bethesda)* **14**, jkad270 (2023).
42. DeSouza, M. M. & Murray, M. K. An estrogen-dependent secretory protein, which shares identity with chitinases, is expressed in a temporally and regionally specific manner in the sheep oviduct at the time of fertilization and embryo development. *Endocrinology* **136**, 2485–2496 (1995).
43. Sendai, Y., Abe, H., Kikuchi, M., Satoh, T. & Hoshi, H. Purification and Molecular Cloning of Bovine Oviduct-Specific Glycoprotein1. *Biol. Reprod.* **50**, 927–934 (1994).
44. Abe, H., Onodera, M. & Sugawara, S. Immunological detection and characterization of an estrus-associated antigen in the goat oviduct. *J. Exp. Zool.* **272**, 134–141 (1995).
45. Hachen, A., Jewgenow, K. & Braun, B. C. Sequence analysis of feline oviductin and its expression during the estrous cycle in the domestic cat (Felis catus). *Theriogenology* **77**, 539–549 (2012).
46. Buhi, W. C., Alvarez, I. M., Choi, I., Cleaver, B. D. & Simmen, F. A. Molecular Cloning and Characterization of an Estrogen-Dependent Porcine Oviductal Secretory Glycoprotein1. *Biol. Reprod.* **55**, 1305–1314 (1996).
47. Verhage, H. et al. Symposium: reproduction in baboons. The baboon oviduct: characteristics of an oestradiol-dependent oviduct-specific glycoprotein. *Hum. Reprod. Update* **3**, 541–552 (1997).
48. Saint-Dizier, M. et al. OVGP1 is expressed in the canine oviduct at the time and place of oocyte maturation and fertilization. *Mol. Reprod. Dev.* **81**, 972–982 (2014).
49. Soleilhavoup, C. et al. Proteomes of the Female Genital Tract During the Oestrous Cycle. *Mol. Cell. Proteom.* **15**, 93–108 (2016).
50. Hoh, R. A., Stowe, T. R., Turk, E. & Stearns, T. Transcriptional program of ciliated epithelial cells reveals new cilium and centrosome components and links to human disease. *PloS one* **7**, e52166 (2012).
51. Paredes, J. et al. Epithelial E- and P-cadherins: role and clinical significance in cancer. *Biochim Biophys. Acta* **1826**, 297–311 (2012).
52. Bui, N.-L.-C. et al. Bad phosphorylation as a target of inhibition in oncology. *Cancer Lett.* **415**, 177–186 (2018).
53. Barton, B. E. et al. Roles of steroid hormones in oviductal function. *Reproduction* **159**, R125–r137 (2020).
54. Jozwik, K. M. & Carroll, J. S. Pioneer factors in hormone-dependent cancers. *Nat. Rev. Cancer* **12**, 381–385 (2012).
55. Crow, J., Amso, N. N., Lewin, J. & Shaw, R. W. Morphology and ultrastructure of fallopian tube epithelium at different stages of the menstrual cycle and menopause. *Hum. Reprod.* **9**, 2224–2233 (1994).
56. Okada, A. et al. Role of foxj1 and estrogen receptor alpha in ciliated epithelial cell differentiation of the neonatal oviduct. *J. Mol. Endocrinol.* **32**, 615–625 (2004).
57. Devoto, L, Soto, E, Magofke, A. M & Sierralta, W Unconjugated Steroids in the Fallopian Tube and Peripheral Blood During the Normal Menstrual Cycle**Supported in part by Grant 79 154 from Programa Latino Americano de Investigación en Reproducción Humana. Fertility Sterility 33, 613–617 (1980).
58. Dong, R. et al. Galectin-3 as a novel biomarker for disease diagnosis and a target for therapy (Review). *Int J. Mol. Med.* **41**, 599–614 (2018
59. Walbrecq, G. et al. Antioxidant cytoprotection by peroxisomal peroxiredoxin-5. *Free Radic. Biol. Med.* **84**, 215–226 (2015).
60. Li, S., Hu, X., Ye, M. & Zhu, X. The prognostic values of the peroxiredoxins family in ovarian cancer. *Biosci. Rep.* **38**, https://doi.org/10.1042/bsr20180667 (2018).
61. Sienko, J., Gaj, P., Czajkowski, K. & Nowis, D. Peroxiredoxin-5 is a negative survival predictor in ovarian cancer. *Ginekol. Pol.* **90**, 1–6 (2019).
62. Agborbesong, E., Zhou, J. X., Li, L. X., Calvet, J. P. & Li, X. Antioxidant enzyme peroxiredoxin 5 regulates cyst growth and ciliogenesis via modulating Plk1 stability. *Faseb j.* **36**, e22089 (2022).
63. Choi, E.-H. & Park, S.-J. TXNIP: A key protein in the cellular stress response pathway and a potential therapeutic target. *Exp. Mol. Med.* **55**, 1348–1356 (2023).
64. Pan, M., Zhang, F., Qu, K., Liu, C. & Zhang, J. TXNIP: A Double-Edged Sword in Disease and Therapeutic Outlook. *Oxid. Med Cell Longev.* **2022**, 7805115 (2022).

65. Borhani, N. et al. Decreased Expression of Proapoptotic Genes Caspase-8- and BCL2-Associated Agonist of Cell Death (BAD) in Ovarian Cancer. *Clin. Ovarian Other Gynecologic Cancer* **7**, 18–23 (2014).
66. Martinelli, D. C. & Fan, C.-M. The Role of Gas1 in Embryonic Development and its Implications for Human Disease. *Cell Cycle* **6**, 2650–2655 (2007).
67. Zarco, N., González-Ramírez, R., González, R. O. & Segovia, J. GAS1 induces cell death through an intrinsic apoptotic pathway. *Apoptosis* **17**, 627–635 (2012).
68. Roche, P. A. & Furuta, K. The ins and outs of MHC class II-mediated antigen processing and presentation. *Nat. Rev. Immunol.* **15**, 203–216 (2015).
69. Wosen, J. E., Mukhopadhyay, D., Macaubas, C. & Mellins, E. D. Epithelial MHC Class II Expression and Its Role in Antigen Presentation in the Gastrointestinal and Respiratory Tracts. *Front Immunol.* **9**, 2144 (2018).
70. Robertson, S. A., Care, A. S. & Moldenhauer, L. M. Regulatory T cells in embryo implantation and the immune response to pregnancy. *J. Clin. Invest* **128**, 4224–4235 (2018).
71. Papi, A. et al. Rhinovirus infection induces major histocompatibility complex class I and costimulatory molecule upregulation on respiratory epithelial cells. *J. Infect. Dis.* **181**, 1780–1784 (2000).
72. Borcherding, F. et al. The CD40-CD40L pathway contributes to the proinflammatory function of intestinal epithelial cells in inflammatory bowel disease. *Am. J. Pathol.* **176**, 1816–1827 (2010).
73. Van Niel, G. et al. Intestinal epithelial exosomes carry MHC class II/peptides able to inform the immune system in mice. *Gut* **52**, 1690–1697 (2003).
74. MacNabb, B. W. & Kline, J. MHC cross-dressing in antigen presentation. *Adv. Immunol.* **159**, 115–147 (2023).
75. Thelemann, C. et al. Interferon-γ induces expression of MHC class II on intestinal epithelial cells and protects mice from colitis. *PLoS One* **9**, e86844 (2014).
76. Westendorf, A. M. et al. CD4+Foxp3+ regulatory T cell expansion induced by antigen-driven interaction with intestinal epithelial cells independent of local dendritic cells. *Gut* **58**, 211–219 (2009).
77. GeoMxWorkflows: GeoMx Digital Spatial Profiler (DSP) data analysis workflows. v. R package version 1.8.0 (2023).
78. Sipes, J. JaredSipesBioE/Sipes-2025-Spatial-Transcriptome-Fallopian-Tube: v1.0 Sipes-2025-Spatial-Transcriptome-Fallopian-Tube [Data set]. Zenodo. https://doi.org/10.5281/zenodo.14884931 (2025).

Acknowledgements

We thank the University of Kansas Medical Center's/University of Kansas Cancer Center's Biospecimen Repository Core Facility (BRCF) for providing human specimens; the BRCF is supported in part by the KU Cancer Center (NCI CCSG-P30 CA168524) and the Kansas Institute for Precision Medicine (NIGMS COBRE-P20 GM130423). This study was supported in part by a grant from the NIH National Cancer Institute (R01 CA260132 to A.K.G.), the Kansas Institute for Precision Medicine (P20 GM130423 to A.K.G.), a graduate student award from the OVERRUN Ovarian Cancer Foundation (to J.S.), a grant from the Ovarian Cancer Research Alliance (to A.K.G.), a grant from the Basser Center for BRCA (to A.K.G.), a grant from the Honorable Tina Brozman Foundation, Inc. (Tina's Wish to A.K.G.), and Predicine Inc.

Author contributions

Conceptualization, Funding Acquisition, Project Administration, A.K.G.; Biostatistics Advisor, L.E.B.; Quality Control and Filtering and Associated R Code, J.S.; Data Normalization and Associated R Code, L.E.B., M.M.R., F.A.; Statistical Analysis and Associated R Code, L.E.B., M.M.R., F.A.; Graphs and Visualizations, J.S.; Methodology, A.K.G., H.B.P., A.M., R.V.P., J.S., S.R., L.E.B., M.M.R., F.A.; Formal Analysis, J.S.; Pathology and Confirmation of Tissue Samples, R.M.; GeoMx DSP Core, J.S., A.M., R.V.P., H.B.P.; Interpretation and analysis, J.S., S.R.; Writing – Original Draft, J.S.; Writing – Review and Editing, J.S., S.R., A.K.G. All authors have read and agreed to the published version of the manuscript.

Competing interests

A.K.G. is a co-founder of Sinochips Diagnostics, serves as a scientific advisory board member to Biovica, Clara Biotech, and Sinochips Diagnostics, and receives research funding from Predicine and VITRAC Therapeutics. The other authors report no conflict of interest.

Additional information

Supplementary information The online version contains supplementary material available at https://doi.org/10.1038/s42003-025-07871-w.

Correspondence and requests for materials should be addressed to Andrew K. Godwin.

Peer review information *Communications Biology* thanks David Huntsman and the other, anonymous, reviewer(s) for their contribution to the peer review of this work. Primary Handling Editors: Ruby Huang and Christina Karlsson Rosenthal.